

NNLO QCD corrections to associated WH production and $H \rightarrow b\bar{b}$ decay

Fabrizio Caola,^{1,*} Gionata Luisoni,^{2,†} Kirill Melnikov,^{3,‡} and Raoul Röntsch^{3,§}

¹*Institute for Particle Physics Phenomenology, Durham University, Durham, UK*

²*Max Planck Institute for Physics, Föhringer Ring 6, 80805 München, Germany*

³*Institute for Theoretical Particle Physics, KIT, Karlsruhe, Germany*

Abstract

We present a computation of the next-to-next-to-leading order (NNLO) QCD corrections to the production of a Higgs boson in association with a W boson at the LHC and the subsequent decay of the Higgs boson into a $b\bar{b}$ pair, treating the b -quarks as massless. We consider various kinematic distributions and find significant corrections to observables that resolve the Higgs decay products. We also find that a cut on the transverse momentum of the W boson, important for experimental analyses, may have a significant impact on kinematic distributions and radiative corrections. We show that some of these effects can be adequately described by simulating QCD radiation in Higgs boson decays to b -quarks using parton showers. We also describe contributions to Higgs decay to a $b\bar{b}$ pair that first appear at NNLO and that were not considered in previous fully-differential computations. The calculation of NNLO QCD corrections to production and decay sub-processes is carried out within the nested soft-collinear subtraction scheme presented by some of us earlier this year. We demonstrate that this subtraction scheme performs very well, allowing a computation of the coefficient of the second order QCD corrections at the level of a few per mill.

*Electronic address: fabrizio.caola@durham.ac.uk

†Electronic address: luisonig@mpp.mpg.de

‡Electronic address: kirill.melnikov@kit.edu

§Electronic address: raoul.roentsch@kit.edu

I. INTRODUCTION

Production of the Higgs boson in association with the W boson $pp \rightarrow WH$ plays an important role in Higgs physics explorations at the LHC [1–4]. For example, it provides direct access to the HWW coupling, which is completely fixed by the gauge symmetry of the Standard Model (SM) but may receive new contributions in its extensions. The WH associated production is known to provide important constraints on such anomalous couplings, see e.g. Ref. [5]. Furthermore, as was pointed out in Ref. [6], by selecting Higgs bosons with relatively high transverse momenta, it is possible to identify and study the decay of a Higgs boson into a $b\bar{b}$ pair with high efficiency. The associated WH production then becomes sensitive to the value of the bottom quark Yukawa coupling which currently is only constrained to within a factor of two relative to its SM value [4, 7].

The importance of associated WH production inspired a large number of computations of higher-order QCD and electroweak (EW) corrections to this process. The next-to-leading order (NLO) QCD and EW corrections to $pp \rightarrow WH$ were computed in Refs. [8] and [9, 10], respectively. NLO QCD and EW fixed order computations were subsequently matched to parton showers in Refs. [11, 12]. The inclusive next-to-next-to-leading order (NNLO) QCD corrections to $pp \rightarrow WH$ can be deduced [13] from the NNLO QCD corrections to the Drell-Yan process $pp \rightarrow W^*$ computed in Refs. [14, 15]. Additional NNLO QCD effects that distinguish associated production from the Drell-Yan process originate from diagrams where the Higgs boson is emitted by loops of top quarks; these effects were computed in Ref. [16] in the large top mass approximation. The numerical program `VH@NNLO`, which allows high-precision computations of the inclusive cross section of associated Higgs boson production, was developed in Ref. [17].

Fully-differential NNLO QCD results for associated WH production were obtained in Refs. [18, 19] using slicing techniques. The NNLO calculation of Ref. [18] was matched to a parton shower in Ref. [20]. NLO QCD corrections to $H \rightarrow b\bar{b}$ decay were combined with NNLO QCD corrections to the $pp \rightarrow WH$ production process in Ref. [21], in the limit of a vanishing b -quark mass, and in Ref. [19], retaining the full m_b dependence. Recently, the computation of Ref. [21] was extended [22] to include the NNLO QCD corrections to $H \rightarrow b\bar{b}$ decay computed earlier in Ref. [23] (see also Ref. [24]), in the limit $m_b \rightarrow 0$. Very

large effects, apparently caused by an improved treatment of radiative corrections in the decay $H \rightarrow b\bar{b}$, were found for some kinematic distributions.

The purpose of this paper is to repeat the computation of Ref. [22]. There are several reasons for doing so. First, it is important to check the appearance of large effects when QCD corrections to decays are included. Also, we note that some peculiar contributions to Higgs decay to a $b\bar{b}$ pair that appear at NNLO QCD for the first time were not considered in the computations of Refs. [23, 24] and we discuss them here.

Second, the type of distributions for which large QCD corrections were found in Ref. [22] are typically pathological at leading order. For example, kinematic requirements can result in certain regions of phase space only being populated at NLO. In these kinematic regions, the NNLO computations provide next-to-leading order corrections so that moderately large effects are not too surprising. In addition, severe cuts on the final state particles imply the appearance of kinematic boundaries that may cause genuine large effects that signal poor convergence of perturbation theory. In general, many of these effects are driven by parton emissions and may be properly described by parton showers. It is then interesting to check to what extent the large radiative corrections found in Ref. [22] can be described by a parton shower applied to $H \rightarrow b\bar{b}$ decay.

Finally, we perform the computation using the local subtraction scheme described recently in Ref. [25]. This scheme is an extension of the original sector-improved residue subtraction scheme developed in Refs. [26, 27]. As we already mentioned, all previous computations of WH production at NNLO QCD were performed using variants of the slicing method and it is interesting to perform the computation using fully local subtractions.

The remainder of the paper is organized as follows. In Section II we briefly review the computational scheme of Ref. [25] with an eye on its application to the production process $pp \rightarrow WH$. In Section III we illustrate the performance of the subtraction scheme by showing numerical results for NNLO QCD corrections to the $pp \rightarrow WH$ process, treating the $H \rightarrow b\bar{b}$ decay at leading order. In Section IV we discuss the generalization of the scheme of Ref. [25] to the decay process $H \rightarrow b\bar{b}$, and point out differences between the production and decay cases. We also present numerical results for the NNLO QCD corrections to the $H \rightarrow b\bar{b}$ decay process, to illustrate the performance of the subtraction scheme in this case as well. Finally, we discuss the phenomenology of the process $pp \rightarrow W(l\nu)H(b\bar{b})$, consistently

including NNLO QCD corrections to both production and decay. We present numerical results for cross sections and selected distributions in Section V and compare them with the approximate treatment of QCD corrections to $H \rightarrow b\bar{b}$ decay using a parton shower in Section VI. We conclude in Section VII.

II. BASICS OF NNLO QCD COMPUTATIONS WITHIN THE NESTED SOFT-COLLINEAR SUBTRACTION FRAMEWORK

The goal of this Section is to review the subtraction scheme for NNLO QCD calculations [25]. We consider the collision of two partons and ask for the fiducial volume cross section defined by an infra-red and collinear-safe observable \mathcal{O} . The fiducial cross section is schematically written as

$$\sigma_f(\mathcal{O}) = \sum_X \int \text{dLips}(\{p_X\}) |\mathcal{M}|^2(\{p_X\}) \mathcal{O}(\{p_X\}), \quad (1)$$

where dLips is the Lorentz-invariant phase space and \mathcal{M} is the amplitude for the process X . In Eq. (1), final states X of increasing multiplicity have to be included to arrive at a high-order result for σ_f . In our case, the leading-order computation includes partonic processes of the type $q\bar{q}' \rightarrow WH$ followed by the decays $H \rightarrow b\bar{b}$ and $W \rightarrow l\bar{\nu}$. Both the production and the $H \rightarrow b\bar{b}$ decay processes are affected by QCD corrections. In this Section we focus on the QCD corrections to WH associated production and consider Higgs decay in the leading-order approximation.

We note that the NNLO QCD corrections to inclusive WH production are known since long ago [13, 16, 17]. The challenge for an exclusive computation is to extract the soft and collinear divergences from, say, a matrix element squared with two additional final state partons relative to the leading-order matrix element, while avoiding integration over momenta of partons that can get resolved.

At next-to-leading order, an understanding of how to do this in full generality using both slicing and subtraction methods was achieved more than twenty years ago [28–31]. Unfortunately, the generalization of these methods to NNLO proved to be difficult and required significant effort. This effort started to pay off in the past two to three years, and a large number of fully-differential NNLO QCD results for important LHC processes has been obtained using different computational methods [26, 27, 32–38].

One of these methods, the so-called sector improved residue-subtraction scheme, was developed in Refs. [26, 27] (see also [33, 39] for related work). Recently, it was shown [25] how to modify the original formulation of the method by exploiting the fact that in QCD soft and collinear singularities are not entangled. This allows one to closely follow the so-called FKS subtraction scheme [30, 31], developed for NLO QCD computations, and perform the required soft and collinear subtractions in a nested way [25]. As a consequence, the computational framework becomes very transparent and, as we show below, numerically efficient. We will illustrate the main idea of Ref. [25] by considering the double-real emission contribution, taking the process $q(p_1)\bar{q}'(p_2) \rightarrow WH + g(p_4)g(p_5)$ as an example. Final states with lower multiplicity can be treated along the same lines although the details can be slightly different. Schematically, we write the corresponding cross section as

$$\sigma_f^{gg}(\mathcal{O}) = \int [dg_4][dg_5]\theta(E_4 - E_5)F_{LM}(1, 2, 4, 5) = \langle F_{LM}(1, 2, 4, 5) \rangle, \quad (2)$$

where

$$F_{LM}(1, 2, 4, 5) = \int d\text{Lips}(p_1 + p_2 - p_4 - p_5 \rightarrow W + H)|\mathcal{M}|^2(\{p\})\mathcal{O}(\{p\}), \quad (3)$$

and

$$[dg_i] = \frac{d^{d-1}p_{g_i}}{(2\pi)^{d-1}2E_{g_i}}\theta(E_{\max} - E_{g_i}) \quad (4)$$

is the phase-space element for a gluon, supplemented with a θ -function that ensures that the gluon energy is bounded from above. Note that we introduced the energy ordering of gluons in Eq. (2) to remove the $1/2!$ identical particles factor.

Our goal is to extract singularities from Eq. (2). These singularities can occur in several ways. For example, the so-called double-soft singularity arises if the energies of the two gluons vanish simultaneously. A single-soft singularity appears if E_5 vanishes at fixed E_4 . Note that due to the energy ordering in Eq. (2) the opposite limit ($E_4 \rightarrow 0$ at fixed E_5) cannot occur. In addition to these soft singularities, there are also collinear singularities that occur when the gluons are emitted along the direction of the incoming quark, incoming anti-quark or if they are emitted collinear to each other.

We need to extract all these singularities in an unambiguous way. We begin with soft singularities. We write

$$\sigma_f^{gg}(\mathcal{O}) = \langle F_{LM}(1, 2, 4, 5) \rangle = \langle \mathcal{S}F_{LM}(1, 2, 4, 5) \rangle + \langle (I - \mathcal{S})F_{LM}(1, 2, 4, 5) \rangle, \quad (5)$$

where \mathcal{S} is an operator that extracts the double-soft¹ singularity from F_{LM} . When the operator \mathcal{S} acts on F_{LM} , it removes the four-momenta of the gluons from both the energy-momentum conserving δ -function inside dLips and the observable \mathcal{O} , and extracts the leading singular behavior from the matrix element squared. The result is well known

$$\mathcal{S}F_{LM}(1, 2, 4, 5) = g_s^2 \text{Eik}(1, 2, 4, 5) F_{LM}(1, 2), \quad (6)$$

where $\text{Eik}(1, 2, 4, 5)$ is the square of the eikonal factor derived in Ref. [36]. It is also given in Ref. [25] using the same notation as we use in this paper.

We deal with the two terms on the right-hand side of Eq. (5) in different ways. In the first term the hard matrix element decouples thanks to Eq. (6) and only the eikonal factor needs to be integrated over the two-gluon phase-space. This integral was performed numerically in Ref. [25]. The second term in Eq. (5) has its double-soft divergences regularized. However, both the $E_5 \rightarrow 0$ divergence at fixed E_4 as well as the collinear divergences are still present there. To take care of them, we repeat the procedure and subtract the $E_5 \rightarrow 0$ singularities at fixed E_4 . We call the corresponding operator S_5 and write

$$\langle (I - \mathcal{S})F_{LM}(1, 2, 4, 5) \rangle = \langle (I - \mathcal{S})(I - S_5)F_{LM}(1, 2, 4, 5) \rangle + \langle S_5(I - \mathcal{S})F_{LM}(1, 2, 4, 5) \rangle. \quad (7)$$

The operator S_5 acting on $F_{LM}(1, 2, 4, 5)$ removes the gluon g_5 from the phase space and the observable and extracts the leading singularity

$$S_5 F_{LM}(1, 2, 4, 5) = \frac{g_s^2}{E_5^2} \left[(2C_F - C_A) \frac{\rho_{12}}{\rho_{15}\rho_{25}} + C_A \left(\frac{\rho_{14}}{\rho_{15}\rho_{45}} + \frac{\rho_{24}}{\rho_{25}\rho_{45}} \right) \right] F_{LM}(1, 2, 4). \quad (8)$$

We use the notation $\rho_{ij} = 1 - \cos\theta_{ij}$ in Eq. (8), where θ_{ij} is the relative angle between partons i and j . Among the two terms on the right hand side in Eq. (7), the first has only collinear divergences and the second has a simplified (i.e. independent of g_5) matrix element. Therefore, the integration over the energy and emission angles of the gluon g_5 can be performed in this term. The remaining matrix element for the process $q\bar{q}' \rightarrow WH + g_4$ can then be treated similarly to a normal NLO computation.

The procedure continues with collinear subtractions that are again applied to the terms on the right hand side in Eq. (7) on top of the soft subtractions shown there. However, an additional step, similar to the energy ordering in Eq. (2), is required. Indeed, we need to

¹ Here we define the double-soft limit as $E_4 \rightarrow 0, E_5 \rightarrow 0$ at fixed E_5/E_4 .

further split the phase space into sectors such that in each of them only a particular type of collinear singularity can occur.

There are two major ingredients to this phase space splitting. First, we partition the phase space into two double-collinear partitions and two triple-collinear partitions. In the two double-collinear partitions, the gluons can only have singularities if $\vec{p}_4||\vec{p}_1, \vec{p}_5||\vec{p}_2$, or if $\vec{p}_4||\vec{p}_2, \vec{p}_5||\vec{p}_1$, respectively. In the two triple-collinear partitions, singularities appear if $\vec{p}_1||\vec{p}_4||\vec{p}_5$ or if $\vec{p}_2||\vec{p}_4||\vec{p}_5$, respectively. We note that in the two latter cases the singularities can also appear if $\vec{p}_4||\vec{p}_5$.

The contributions of the double-collinear partitions can be computed right away since all singular limits are uniquely established. The situation is more complex for the triple-collinear partitioning where this is not the case. Indeed, in triple-collinear configurations we need to consider the two cases of the gluons being either close or well-separated in rapidity. To this end, we further partition the phase space into four sectors. Taking as an example the $\vec{p}_1||\vec{p}_4||\vec{p}_5$ partitioning, we introduce four sectors according to the following formula

$$1 = \theta\left(\rho_{51} < \frac{\rho_{41}}{2}\right) + \theta\left(\frac{\rho_{41}}{2} < \rho_{51} < \rho_{41}\right) + \theta\left(\rho_{41} < \frac{\rho_{51}}{2}\right) + \theta\left(\frac{\rho_{51}}{2} < \rho_{41} < \rho_{51}\right). \quad (9)$$

Note that this splitting is largely arbitrary. The important point is that in each of the four sectors only a well-defined type of singular collinear limit can occur; by choosing an appropriate parametrization, these singularities can be resolved and isolated. The nested subtraction of these collinear limits can then be performed, similar to what we discussed in connection with the soft limits. A convenient phase-space parametrization for each of the four sectors can be found in Ref. [26].

A detailed discussion of this approach can be found in Ref. [25] which an interested reader should consult. Below, we list a few aspects of the current computation that go beyond that reference.

- We extend the computation of Ref. [25] by including the $qg \rightarrow WH + q'g$ partonic channel. The difference with the quark-anti-quark annihilation channel is that the quark-gluon channel appears for the first time at NLO and, therefore, to obtain the result relevant for the NNLO computation, we only need to include one-loop corrections to this channel and consider one additional gluon in the final state. There are no

conceptual differences with the computations described in Ref. [25] and, similarly to that reference, compact formulas are obtained for the NNLO contribution of the quark-gluon channel. In our implementation, we used a slightly different parametrization of the phase space compared to Ref. [25] making use of the fact that there are no single-soft singularities related to quark emission.

- We compute all the channels with an additional quark-anti-quark pair in the final state $q\bar{q}' \rightarrow WH + q_1\bar{q}_2$. If the quark-anti-quark pair comes from gluon splitting, the corresponding process has a double-soft singularity that is different from the one described above; the integral of the respective eikonal factor has to be computed anew.
- We compute the contribution of the $gg \rightarrow WH + q\bar{q}'$ channel. This channel has simple collinear divergences and their extraction is straightforward.
- We include the NNLO contributions to the associated production $pp \rightarrow WH$ where the Higgs boson is emitted from a loop of virtual top quarks. These include two-loop corrections to the $q\bar{q} \rightarrow WH$ partonic process, as well as one-loop corrections to the $q\bar{q} \rightarrow WH + g$ process. These finite contributions were first computed in Ref. [16], where they were referred to as V_I and R_I , respectively. We take the amplitude for V_I in an expansion in $1/m_{\text{top}}$ and the amplitude for R_I with the exact mass dependence from Refs. [16, 19].

III. ASSOCIATED WH PRODUCTION

In this Section we present results of the computation of the NNLO QCD corrections to the process $pp \rightarrow W(l\nu)H(b\bar{b})$ at the center-of-mass energy $\sqrt{s} = 13$ TeV. We compute LO, NLO and NNLO cross sections and distributions *always* using NNPDF3.0 NNLO parton distribution functions [40]. We use the numerical value of the strong coupling constant provided by the PDF set, with $\alpha_s(m_Z) = 0.118$.

The Higgs and the W boson masses are taken to be 125 GeV and 80.398 GeV, respectively. The mass of the top quark is set to 173.2 GeV. The decays of the Higgs boson and of the W boson are included in the narrow width approximation. In this Section, we consider the $H \rightarrow b\bar{b}$ decay at LO only. The width of the W boson is $\Gamma_W = 2.1054$ GeV. The

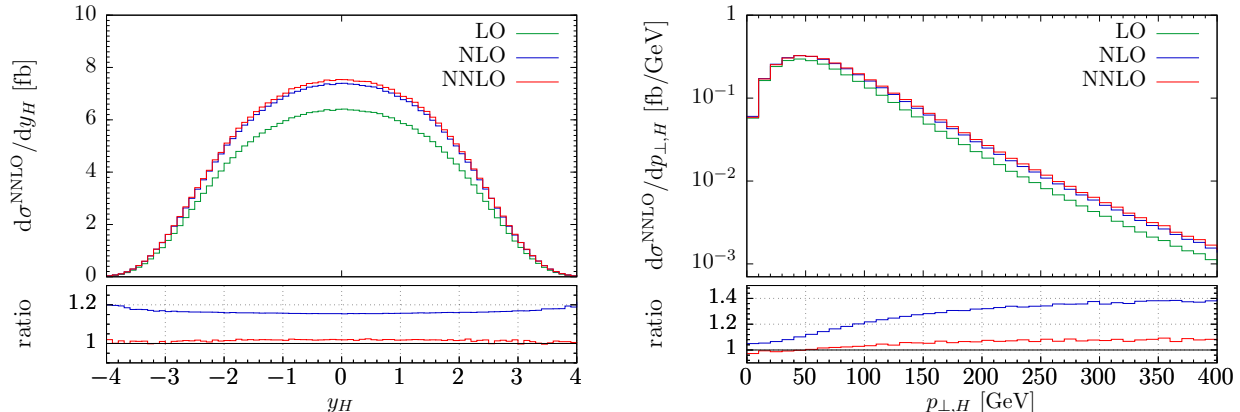


Figure 1: Results for the rapidity and the transverse momentum distributions of the Higgs boson. Upper panes – results in consecutive orders of perturbation theory. Lower panes – ratios of NLO to LO and NNLO to NLO. The renormalization and factorization scales are set to $\mu = M_{WH}$. In this plot, LO, NLO and NNLO results are all computed with NNLO PDFs, see text for detail.

Fermi constant is $G_F = 1.16639 \times 10^{-5} \text{ GeV}^{-2}$, and we take $\sin^2 \theta_W = 0.2226459$ as the sine squared of the weak mixing angle. We also approximate the CKM matrix by an identity matrix. For the decay of the Higgs boson, we take the b -quark Yukawa coupling to be $y_b = \sqrt{2} m_b(m_H)/v = 0.0176$, which corresponds to $m_b(m_H) = 3.07 \text{ GeV}$. We consider only the leading term in m_b , which at this order corresponds to treating b -quarks as massless particles but with a non-vanishing Yukawa coupling. Finally, the Higgs boson width is taken to be $\Gamma_H = 4.165 \text{ MeV}$.

We employ dynamic renormalization and factorization scales that we take to be proportional to the invariant mass of the WH system M_{WH} . We compute the NNLO QCD corrections for three values of the scales $\mu = M_{WH}/2$, $\mu = M_{WH}$ and $\mu = 2M_{WH}$, while keeping the scale of the b -quark Yukawa coupling fixed to m_H .

We report our results for W^+ and W^- production in Table I. NLO QCD corrections increase the leading order cross section by about 15%; the NNLO QCD corrections increases the NLO cross sections by an additional 2%. We note that the scale dependence of the NNLO cross sections is below a percent. Therefore, it is both completely negligible and unlikely to be a reliable estimate of the actual theory uncertainty. This issue has been discussed at length in Ref. [41], and we do not comment on it here. Ratios of W^+ and W^- cross sections stay close to 1.57 – 1.58, independent of both the order of perturbation theory and the choice of

	$pp \rightarrow W^+H \rightarrow l^+\nu b\bar{b}$			$pp \rightarrow W^-H \rightarrow l^-\bar{\nu} b\bar{b}$		
	$\mu = M_{WH}/2$	$\mu = M_{WH}$	$\mu = 2M_{WH}$	$\mu = M_{WH}/2$	$\mu = M_{WH}$	$\mu = 2M_{WH}$
σ_{LO} (fb)	44.340(5)	45.748(6)	46.834(6)	28.207(5)	29.158(5)	29.890(5)
σ_{NLO} (fb)	53.475(6)	53.286(6)	53.284(7)	33.867(5)	33.773(5)	33.805(5)
σ_{NNLO} (fb)	54.498(13)	54.401(18)	54.378(10)	34.452(5)	34.402(5)	34.397(5)

Table I: Results for $pp \rightarrow W^+H \rightarrow l^+\nu b\bar{b}$ (left) and $pp \rightarrow W^-H \rightarrow l^-\bar{\nu} b\bar{b}$ (right). Higgs boson emissions off the top quark loops are included. Higgs decays are accounted for at the LO approximation. See text for details.

the factorization and the renormalization scales. We have cross-checked all these numbers against VH@NNLO [17] and found perfect agreement.

As the next step, we study the NNLO corrections in more detail, focusing on the case of W^-H production.² The NNLO QCD *contributions* to the W^-H production cross section without the finite contributions R_I and V_I describing Higgs boson emission off a top quark loop read

$$\delta\sigma_{\text{NNLO}}^{\text{no top loops}} = \{0.0937(7), 0.2193(7), 0.2464(7)\} \text{ fb}, \quad (10)$$

for the renormalization and factorizations scales $\mu = \{M_{WH}/2, M_{WH}, 2M_{WH}\}$ respectively. Note that the numerical integration error on the NNLO *coefficients* is just a few per mill. Also in this case, full agreement with Ref. [17] was found. The fact that our computational method is capable of delivering results at this level of numerical precision for the NNLO QCD coefficients has already been noticed in the calculation reported in Ref. [25]. However, since the calculation of Ref. [25] was performed for a simplified case, it is gratifying to see that this feature persists in a more complex situation where all the different partonic channels are included in the calculation, and significant numerical cancellations between their contributions occur.

NNLO QCD corrections to kinematic distributions can also be computed with a high degree of numerical stability. In Fig. 1 we display the Higgs boson rapidity and transverse momentum distributions in consecutive orders of QCD perturbation theory, for the case of W^-H production. In the lower panels of Fig. 1 we also display ratios of NLO to LO and NNLO to

² Results for W^+H production show a similar qualitative behavior.

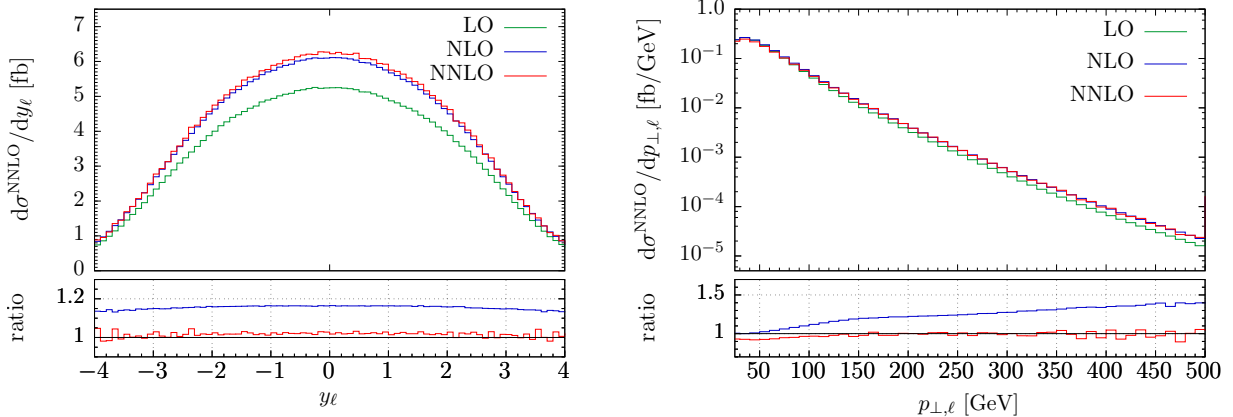


Figure 2: Results for rapidity and transverse momentum distributions of the charged lepton from the decay of a W^- boson. Upper panes – results in consecutive orders of perturbation theory. Lower panes – ratios of NLO to LO and NNLO to NLO. The renormalization and factorization scales are set to $\mu = M_{WH}$. In this plot, LO, NLO and NNLO results are all computed with NNLO PDFs, see text for detail.

NLO distributions. In Fig. 2 we show results for the rapidity and the transverse momentum distributions of the charged lepton from the decay of the W boson. The numerical stability of these computations is clearly very good.

IV. HIGGS DECAY TO A PAIR OF BOTTOM QUARKS

In this Section, we discuss a fully exclusive computation of NNLO QCD corrections to Higgs boson decay to a $b\bar{b}$ pair. Such computations were performed in Refs. [23, 24]. Unfortunately, both of these references did not consider an interesting subtlety related to this decay that we will explain first.

We consider the Standard Model Lagrangian, integrate out the top quark and neglect the interaction of the Higgs boson with quarks of the first two generations. Interactions of the Higgs boson with hadronic constituents are then described by an effective Lagrangian

$$\mathcal{L} = -C_1 \frac{\alpha_s}{12\pi v} G_{\mu\nu}^a G^{a,\mu\nu} H - C_2 \frac{m_b}{v} H b\bar{b}. \quad (11)$$

The two terms in Eq. (11) refer to interactions of Higgs bosons with gluons and b -quarks, respectively. The first term originates from the $Ht\bar{t}$ interaction and, therefore, is proportional

to the Higgs-top Yukawa coupling; the second term is proportional to the Higgs-bottom Yukawa coupling.

The two constants $C_{1,2}$ in Eq. (11) are the Wilson coefficients of the corresponding operators. Their perturbative expansions in the strong coupling constant – to the order relevant to us – read (see e.g. [42])

$$C_1 = -1 + \mathcal{O}(\alpha_s), \quad C_2 = 1 + \left(\frac{\alpha_s}{2\pi}\right)^2 \left[\frac{10}{9} - \frac{4}{3} \log \frac{\mu^2}{m_t^2}\right] + \mathcal{O}(\alpha_s^3). \quad (12)$$

The computation of NNLO QCD corrections to Higgs boson decay to two b -quarks reported in Refs. [23, 24] was performed under a tacit assumption $C_1 = 0$ and $C_2 = 1$. As we explain below, $C_1 \neq 0$ leads to additional contributions to Higgs decay to $b\bar{b}$ starting at NNLO. In the limit of a small b -quark mass, these contributions scale like $\sim y_b m_b/v \sim m_b^2/v^2$, so they are parametrically indistinguishable from terms proportional to y_b^2 coming from C_2 alone. As a consequence, they should be included in an NNLO computation. However, before discussing this point, we repeat the computation of the decay $H \rightarrow b\bar{b}$ reported in Refs. [23, 24] by setting $C_1 = 0$, $C_2 = 1$.

A. Higgs decay to a $b\bar{b}$ pair: contribution proportional to bottom Yukawa coupling squared

In this subsection, we compute NNLO QCD corrections to the decay $H \rightarrow b\bar{b}$ in the approximation $C_1 = 0$. We treat b -quarks as massless but with a non-vanishing Yukawa coupling to the Higgs boson. The generalization of the computational method described in Ref. [25] to this case is straightforward. Since the collinear renormalization of parton distribution functions is obviously not needed in this case, the computation is simpler and the final formulas for the NNLO QCD corrections are more compact. There are, however, a few subtleties, which we point out in this Section.

First, as we already mentioned, we work in the approximation of massless b -quarks. This means that the only place where the b -quark mass appears is in the Yukawa coupling. We renormalize the Yukawa coupling in the $\overline{\text{MS}}$ -scheme at the scale $\mu = m_H$. It is well-known from the computation of the inclusive rate that this choice of the renormalization scale reduces the magnitude of QCD radiative corrections that are very large otherwise [43].

Second, integrals of the double-soft eikonal factors are identical to the production case and can be re-used in the $H \rightarrow b\bar{b}$ computation. Other numerical components of the computation, i.e. integrals of the triple-collinear splitting functions, are different from the production case but they actually become simpler.³

Third, it turns out that the calculation of *the double-collinear contributions* is non-trivial for the decay kinematics. This is in stark contrast to the computation of the NNLO QCD corrections to the production case where the double-collinear contribution is among the simplest. The reason for this difference is as follows. The double-collinear contributions refer to sectors where collinear singularities appear if, say, the gluon g_4 is emitted collinear to the b -quark and the gluon g_5 is emitted collinear to the \bar{b} -anti-quark. To extract collinear divergences in this case, it is convenient to choose cosines of the relative angles between \vec{p}_b and \vec{p}_4 and between $\vec{p}_{\bar{b}}$ and \vec{p}_5 as independent kinematic variables. For the decay case, we work in the rest frame of the Higgs boson. Hence, in contrast to the production case, the directions of \vec{p}_b and $\vec{p}_{\bar{b}}$ are not fixed. It then appears to be non-trivial to use the two angles as independent variables and to have the phase space properly simplify in soft and collinear limits, while also satisfying the constraint $p_H = p_4 + p_5 + p_b + p_{\bar{b}}$. Nevertheless, this can be done and we will present the corresponding formulas in a separate publication. Here, we only note that this complexity is a particular feature of the process at hand. Since the Born process $H \rightarrow b\bar{b}$ involves too few particles, the momentum conservation constraint makes it difficult to find a parametrization in terms of the two angles discussed above. For more complicated decay processes, for example for Z decays to three jets, this issue is not present.

The last point concerns the contribution of the $b\bar{b}b\bar{b}$ final state to the decay rate of the Higgs boson. This final state is different from everything that we considered so far because we cannot say *a priori* which of the two $b\bar{b}$ pairs comes from the Higgs vertex and which from the $g^* \rightarrow b\bar{b}$ splitting. Without this information, we cannot separate the phase space into a hard part and a radiation part, which is central for the method of Ref. [25]. To get around this problem, we use the symmetry of the process $H \rightarrow b\bar{b}b\bar{b}$ with respect to the permutations of the two b -quarks and the two \bar{b} -anti-quarks and split the matrix element into a part that is equivalent to the singlet component $H \rightarrow b\bar{b} + q\bar{q}$, $q \neq b$, and an identical quark interference contribution. In each of the interference contributions, there is either a

³ They are functions of a momentum fraction in the production case and just numbers in the decay case.

quark line or an anti-quark line that always originates from the Higgs decay vertex. We assign this line to belong to the hard phase space. The remaining lines can originate either from the Higgs decay vertex or from the $g^* \rightarrow b\bar{b}$ splitting. Which line belongs to the hard phase space and which one to the radiative phase space is a matter of choice at this point. The interference terms only contain a purely triple-collinear singularity. It corresponds to the interference term in the non-singlet triple-collinear splitting function [44] and can be easily extracted and integrated numerically.

We continue by presenting some numerical results of the calculation. Again, our goal in this Section is not to discuss phenomenology of the Higgs boson decay to a $b\bar{b}$ pair but to show that our method is capable of producing high-precision results.

The numerical computation yields the following result for the decay rate of the Higgs boson to a $b\bar{b}$ pair

$$\Gamma(H \rightarrow b\bar{b}) = \Gamma_{\text{LO}} \left[1 + \left(\frac{\alpha_s}{2\pi}\right) 11.3333(16) + \left(\frac{\alpha_s}{2\pi}\right)^2 116.68(8) + \dots \right], \quad (13)$$

where $\Gamma_{\text{LO}} = 3y_b^2 m_H / (16\pi) = 3m_b^2(m_H)m_H / (8\pi v^2)$. The value of the Yukawa coupling constant has already been discussed in the previous Section. The renormalization scale for the strong coupling constant is set to the mass of the Higgs boson.

It is instructive to compare Eq. (13) with the results of an analytic computation [45]. The analytically-known two-loop coefficient evaluates to 116.59... which is in better than per mill agreement with the result of the numerical computation shown in Eq. (13).

It is also interesting to compute jet rates in $H \rightarrow b\bar{b}$ decay since such, more exclusive, calculations provide a stronger test of the numerical stability of the method. Similar to Ref. [24], we use the JADE clustering algorithm with $y_{\text{cut}} = 10^{-2}$ to define jets.⁴ We obtain

$$\begin{aligned} \Gamma_{2j} &= \Gamma_{\text{LO}} \left[1 - 27.176(3) \left(\frac{\alpha_s}{2\pi}\right) - 1240.78(21) \left(\frac{\alpha_s}{2\pi}\right)^2 + \mathcal{O}(\alpha_s^3) \right], \\ \Gamma_{3j} &= \Gamma_{\text{LO}} \left[38.509(3) \left(\frac{\alpha_s}{2\pi}\right) + 980.61(10) \left(\frac{\alpha_s}{2\pi}\right)^2 + \mathcal{O}(\alpha_s^3) \right], \\ \Gamma_{4j} &= 376.784(8) \left(\frac{\alpha_s}{2\pi}\right)^2 \Gamma_{\text{LO}} + \mathcal{O}(\alpha_s^3). \end{aligned} \quad (14)$$

⁴ Following Ref. [24], we define the JADE distance as $y_{ij} = (p_i + p_j)^2$.

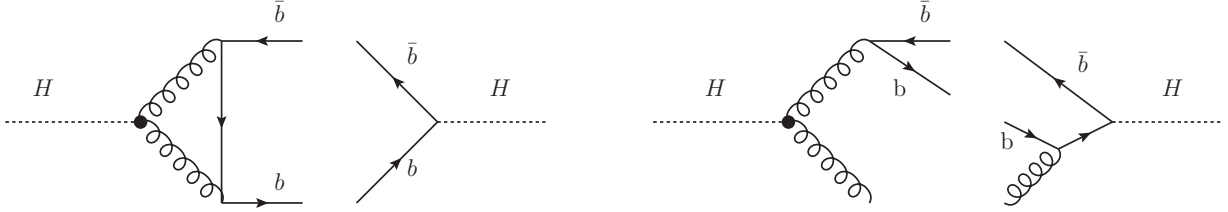


Figure 3: Illustrative interference diagrams that contribute to the $H \rightarrow b\bar{b}$ decay rate for $C_1 \neq 0$. See text for details.

The sum of the exclusive jet rates in Eq. (14) gives the total decay rate; computing this sum, we obtain

$$\Gamma(H \rightarrow b\bar{b}) = \Gamma_{2j} + \Gamma_{3j} + \Gamma_{4j} = \Gamma_{\text{LO}} \left[1 + \left(\frac{\alpha_s}{2\pi} \right) 11.3334(41) + \left(\frac{\alpha_s}{2\pi} \right)^2 116.62(23) + \dots \right]. \quad (15)$$

Comparing the inclusive computation shown in Eq. (13) with the sum of exclusive jet rates in Eq. (15), we find perfect agreement although the integration error is somewhat larger in the latter case.

B. Additional contributions to Higgs decay proportional to top Yukawa coupling

We mentioned above that a non-vanishing Wilson coefficient C_1 gives rise to additional contributions to $H \rightarrow b\bar{b}$ decays starting at NNLO in QCD, which were not considered in previous fully-differential calculations [23, 24]. We describe these contributions in more detail in this subsection. These contributions are of the interference type: an amplitude where the Higgs boson decays to two (real or virtual) gluons that later turn into bottom quarks interferes with an amplitude where the Higgs boson decays directly to bottom quarks and gluons.

Some of these contributions are shown in Fig. 3. They are proportional to the product of two Wilson coefficients $C_1 C_2$ and, therefore, to the *first power* of the b -quark Yukawa coupling, at variance with contributions to $H \rightarrow b\bar{b}$ decay considered in the previous subsection. However, angular momentum conservation implies that diagrams in Fig. 3 can interfere only if a helicity flip occurs on one of the b -quark lines; effectively, this helicity flip and the Wilson coefficient C_1 provide another factor m_b/v , making the overall scaling of these

interference contributions with the b -quark mass identical to what we have seen in the previous subsection.

These contributions are soft and collinear finite for $m_b \neq 0$. Indeed, taking the real emission contribution as an example, it is easy to see that the collinear singularity associated with the splitting $g^* \rightarrow b\bar{b}$ is regulated because the gluon invariant mass should exceed $2m_b$. Similar considerations ensure that the virtual diagram shown in Fig. 3 has no soft and collinear divergences for finite m_b as well.

However, since the calculation in the previous subsection was performed with massless b -quarks, we would like to compute the diagrams shown in Fig. 3 in the same approximation. Unfortunately, doing so leads to problems. Indeed, if we factor out one power of m_b caused by the helicity flip, the reduced matrix element has peculiar soft and collinear limits in the $m_b = 0$ approximation, that are typically not present in QCD amplitudes at leading power. For example, it develops a logarithmic singularity when a *single* b -quark becomes soft.

The validity of the massless approximation assumes that the logarithmic dependence on the b -quark mass cancels out in infra-red safe quantities. It is easy to see, however, that this cancellation does not take place for the interference contributions, and it is not possible to give a proper inclusive definition of this process in the massless approximation. Indeed, the logarithmic mass dependence cancels between the diagrams in Fig. 3 *and* similar diagrams with a b -mediated Higgs decay into gluons. One could try to circumvent this problem by regulating the collinear singularity related to $g^* \rightarrow b\bar{b}$ with a flavored jet algorithm, e.g. the one in Ref. [46]. This would trade the logarithmic dependence on the b -quark mass for a logarithmic sensitivity to a jet radius R . However, even this does not solve the problem completely as the single-soft quark singularity is *not* regulated by the jet algorithm of Ref. [46].

It is clear that a proper description of the interference contributions requires a computation with fully massive b -quarks. In its absence, we estimate the order of magnitude of these effects by simply imposing restrictions on the phase space of the b -quarks and gluons that reproduce the leading logarithmic terms. We find that these contributions may change the NNLO corrections to the inclusive Higgs decay rate shown in Eq. (13) by up to $\mathcal{O}(30\%)$. Using the same setup in the fiducial region that will be discussed in the next Section, we find that this interference contribution is somewhat reduced. Since their impact on the decay

rate appears to be limited, we will omit these terms from the phenomenological analysis in the next Section but we stress that it is important to understand them better. As we explained, this will require a fully-differential computation of the Higgs decay to massive bottom pairs at NNLO. We leave this for future investigations.

V. THE PHYSICAL PROCESS

We are now in position to discuss the physical process $pp \rightarrow W(l\nu)H(b\bar{b})$, including QCD corrections to both production and decay. Given the results of the preceding Sections, it is straightforward to do so. The only subtlety is how to treat the Higgs boson decay width that appears in the cross section in the narrow width approximation. We write

$$d\sigma_{WH(bb)} = d\sigma_{WH} \times \frac{d\Gamma_{bb}}{\Gamma_H} = \text{Br}(H \rightarrow b\bar{b}) \times d\sigma_{WH} \times \frac{d\Gamma_{bb}}{\Gamma_{bb}}. \quad (16)$$

We note that in the approximation of massless b -quarks, the Higgs boson decay rate to a $b\bar{b}$ pair and *therefore the Higgs branching ratio to a $b\bar{b}$ -pair* subtly depends on the definition of a b -quark. However, the effect on the total decay rate is relatively small, as discussed in the previous Section, and we set $C_1 = 0$ for the phenomenological studies in this paper. We use $\text{Br}(H \rightarrow b\bar{b}) = 0.5824$ [41] as a fixed quantity, not subject to an α_s expansion.

To define an expansion of Eq. (16) in α_s , we follow Ref. [22], write the production cross section and the decay width to $b\bar{b}$ as an expansion in α_s

$$d\sigma_{WH} = \sum_{i=0}^{\infty} d\sigma_{WH}^{(i)}, \quad d\Gamma_{bb} = \sum_{i=0}^{\infty} d\Gamma_{bb}^{(i)}, \quad (17)$$

and introduce

$$d\gamma^{(i)} = \frac{\sum_{j=0}^i d\Gamma_{bb}^{(j)}}{\sum_{j=0}^i \Gamma_{bb}^{(j)}}. \quad (18)$$

Note that $\int d\gamma^{(i)} = 1$, provided that the integration goes over the unrestricted phase space.

Using this notation, we define the physical cross sections computed through different orders in QCD perturbation theory

$$\begin{aligned} d\sigma_{WH(bb)}^{\text{LO}} &= \text{Br}(H \rightarrow b\bar{b}) d\sigma^{(0)} d\gamma^{(0)}, \\ d\sigma_{WH(bb)}^{\text{NLO}} &= \text{Br}(H \rightarrow b\bar{b}) [d\sigma^{(0)} d\gamma^{(1)} + d\sigma^{(1)} d\gamma^{(0)}], \\ d\sigma_{WH(bb)}^{\text{NNLO}} &= \text{Br}(H \rightarrow b\bar{b}) [d\sigma^{(0)} d\gamma^{(2)} + d\sigma^{(1)} d\gamma^{(1)} + d\sigma^{(2)} d\gamma^{(0)}]. \end{aligned} \quad (19)$$

In addition, for comparison with the previous computations of Refs. [19, 21], it is convenient to introduce an approximate NNLO cross section that includes NNLO corrections to the production process but only NLO corrections to the decay. It reads

$$d\sigma_{WH(b\bar{b})}^{\text{NNLO,approx}} = \text{Br}(H \rightarrow b\bar{b}) [d\sigma^{(0)} d\gamma^{(1)} + d\sigma^{(1)} d\gamma^{(0)} + d\sigma^{(2)} d\gamma^{(0)}]. \quad (20)$$

We are now in a position to discuss the results of the computation. To define the $W(l\nu)H(b\bar{b})$ final state, we reconstruct b -jets using the infra-red safe flavor- k_t jet algorithm [46]⁵ with $\Delta R = 0.5$ and require that an event should contain at least one b -jet and one \bar{b} -jet with

$$|\eta_{j_b}| < 2.5, \quad p_{\perp,j_b} > 25 \text{ GeV}. \quad (21)$$

An identified light (non- b) jet is required to have a transverse momentum $p_{\perp} > 25$ GeV as well but no pseudo-rapidity cut is applied in this case. In addition, we impose the following cuts on the pseudorapidity and transverse momentum of the charged lepton

$$|\eta_l| < 2.5, \quad p_{\perp,l} > 15 \text{ GeV}. \quad (22)$$

Finally, following the experimental analyses, we may impose an additional requirement that the vector boson has a transverse momentum $p_{\perp,W} > 150$ GeV. We use parton distribution functions NNPDF3.0 as in Section III. However, at variance with the calculation reported there, here we employ LO, NLO and NNLO PDFs to compute LO, NLO and NNLO cross sections, respectively.

We begin by presenting the fiducial volume cross sections for the process $pp \rightarrow W(l\nu)H(b\bar{b})$ at the 13 TeV LHC, at various orders in perturbative QCD. The W^+ case has already been studied in Ref. [22]. For this reason here we focus on the W^- case. Without the cut on $p_{\perp,W}$, we find

$$\begin{aligned} \sigma_{\text{fid},W^-}^{\text{LO}} &= 15.50_{-0.56}^{+0.44} \text{ fb}, & \sigma_{\text{fid},W^-}^{\text{NLO}} &= 16.13_{+0.20}^{-0.09} \text{ fb}, \\ \sigma_{\text{fid},W^-}^{\text{NNLO}} &= 15.20_{+0.11}^{-0.08} \text{ fb}, & \sigma_{\text{fid},W^-}^{\text{NNLO,approx}} &= 16.56_{+0.16}^{-0.11} \text{ fb}. \end{aligned} \quad (23)$$

⁵ We are grateful to G. Salam for providing us with his private implementation of the algorithm [46] within the **FastJet** framework [47].

Imposing the cut on the transverse momentum of the W boson $p_{\perp,W} > 150$ GeV, we obtain

$$\begin{aligned}\sigma_{\text{fid},W^-}^{\text{LO}} &= 2.027_{+0.006}^{-0.013} \text{ fb}, & \sigma_{\text{fid},W^-}^{\text{NLO}} &= 2.381_{+0.055}^{-0.041} \text{ fb}, \\ \sigma_{\text{fid},W^-}^{\text{NNLO}} &= 2.357_{+0.018}^{-0.026} \text{ fb}, & \sigma_{\text{fid},W^-}^{\text{NNLO,approx}} &= 2.516_{+0.025}^{-0.030} \text{ fb}.\end{aligned}\tag{24}$$

For the cross sections in Eqs. (23,24) the central value corresponds to the factorization and renormalization scales *in the production process* set to the invariant mass of the WH system. The uncertainties are obtained by changing simultaneously the renormalization and factorization scales in the production process by a factor of two, $\mu_R = \mu_F = \{1/2, 1, 2\} \times m_{WH}$. As we said already, this is most likely an underestimate of the total theory uncertainty, but this issue has already been discussed at length in the literature (see e.g. [41]) and it is not the point of our study. Consequently, we do not comment on it any further and, in what follows, we only show distributions for the central scale choice. For the decay process, we always use the scale $\mu = m_H$.

The results for the fiducial cross sections Eqs. (23,24) show that NLO QCD effects are larger if a transverse momentum cut is imposed on the W boson. This is expected since the W boson can evade this cut by recoiling against additional radiation which appears at NLO. The approximate NNLO results, which include NNLO corrections to the production process only, show a similar effect: this cross section is about 3% higher than the NLO cross section without the $p_{\perp,W}$ cut, but about 6% higher when this cut is imposed. Including Higgs decay at NNLO decreases the approximate cross section by about 9% without the $p_{\perp,W}$ cut, and 7% in the presence of this cut. Therefore there are cancellations between corrections to the production and decay sub-processes, that make the size of the full NNLO QCD corrections quite sensitive to the value of the $p_{\perp,W}$ cut.

We now turn to differential distributions. We begin by identifying the $b\bar{b}$ system comprised of a b -jet and a \bar{b} -jet whose invariant mass best approximates the mass of the Higgs boson, and consider the invariant mass $m_{b\bar{b}}$ distribution of this $b\bar{b}$ system. Since we work in the narrow width approximation, at leading order this distribution is described by a delta-function $\delta(m_{b\bar{b}}^2 - m_H^2)$. At next-to-leading order, this situation changes: a gluon emitted in the Higgs boson decay can decrease the invariant mass of the $b\bar{b}$ system while a gluon emitted in the production process can increase it. Hence, the $m_{b\bar{b}}$ distribution has tails both above

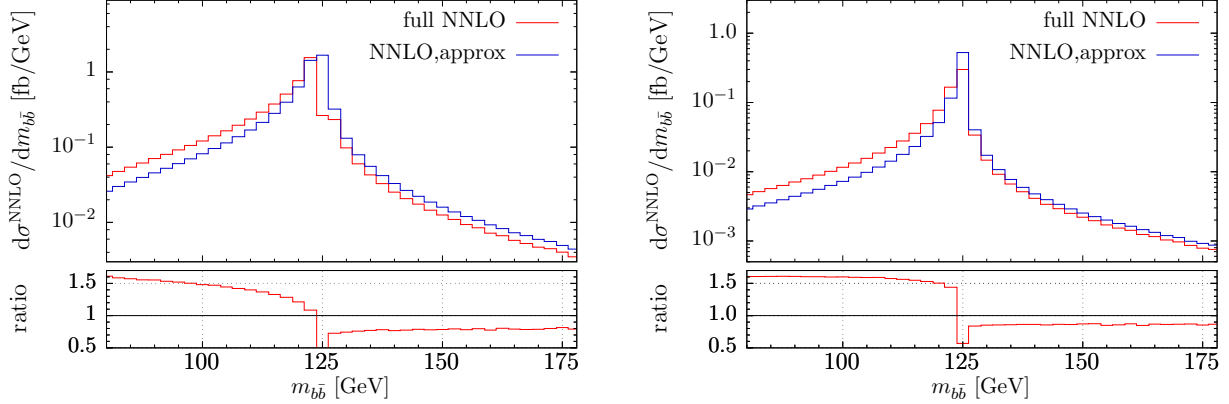


Figure 4: The invariant mass of a b -jet and a \bar{b} -jet that best approximates the Higgs boson mass. Left pane – without the p_{\perp}^W cut, right pane – with the $p_{\perp}^W > 150$ GeV cut. Lower panes – ratio of full NNLO to approximate NNLO. The renormalization and factorization scales are set to $\mu_R = \mu_F = M_{WH}$ for the production process and to $\mu_R = m_H$ for the decay process. See text for further details.

and below $m_{b\bar{b}} = m_H$ that start to appear if the next-to-leading order correction to either production or decay is included in the computation. In Fig. 4 we compare predictions for this observable obtained using full and approximate NNLO computations, defined in Eqs. (19,20), respectively. We study this observable both without (left) and with (right) the cut on the W boson transverse momentum $p_{\perp,W} > 150$ GeV. It is seen from Fig. 4 that the application of this cut affects the shape of $m_{b\bar{b}}$ distribution in a minor way. For example, in both cases, full NNLO results deplete the distribution at $m_{b\bar{b}} > m_H$ and enhance the distribution at $m_{b\bar{b}} < m_H$ relative to approximate NNLO predictions. Since the full NNLO provides a better description of the radiation in the decay, compared to the approximate NNLO, and since radiation in the decay predominantly reduces $m_{b\bar{b}}$, this re-shaping is not unexpected. However, the magnitude of this $\mathcal{O}(\alpha_s^2)$ effect – $\mathcal{O}(60\%)$ correction at $m_{b\bar{b}} \sim 80$ GeV and $\mathcal{O}(-15\%)$ at $m_{b\bar{b}} > m_H$ – is somewhat surprising. We note that similarly large corrections have also been observed in Ref. [22].

To understand what causes these large effects, we split the difference between approximate NNLO and full NNLO into two terms – NNLO radiation in the decay (NNLO_{dec}) and NLO radiation in the production followed by the NLO radiation in the decay ($\text{NLO}_{\text{prod}} \times \text{NLO}_{\text{dec}}$).

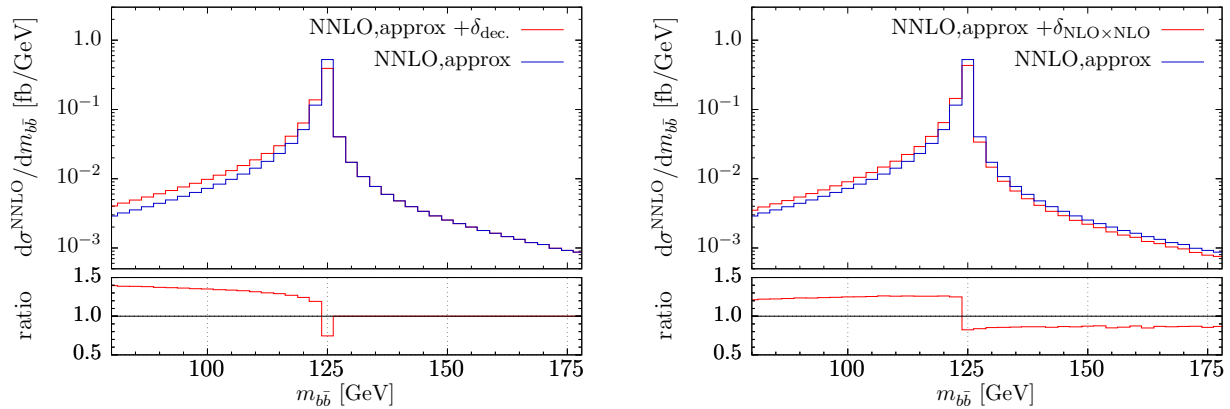


Figure 5: The invariant mass of a b -jet and a \bar{b} -jet that best approximates the Higgs boson mass. The $p_{\perp}^W > 150$ GeV cut is applied. Left pane: only NNLO corrections to decay are included. Right pane: NLO corrections to the production and NLO corrections to the decay are included. Lower panes – ratio to approximate NNLO. See text for further details.

We define

$$\begin{aligned}\delta_{\text{dec.}} &= \text{Br}(H \rightarrow b\bar{b}) d\sigma^{(0)} (d\gamma^{(2)} - d\gamma^{(1)}), \\ \delta_{\text{NLO}\times\text{NLO}} &= \text{Br}(H \rightarrow b\bar{b}) d\sigma^{(1)} (d\gamma^{(1)} - d\gamma^{(0)}),\end{aligned}\tag{25}$$

such that $d\sigma_{WH(b\bar{b})}^{\text{NNLO,approx}} + \delta_{\text{dec.}} + \delta_{\text{NLO}\times\text{NLO}} = d\sigma_{WH(b\bar{b})}^{\text{NNLO}}$. We display the two distributions in Fig. 5. As we said already, the radiation in the decay does not populate the $m_{b\bar{b}}$ region to the right of m_H , so that the $\mathcal{O}(-15\%)$ correction at such values of the $b\bar{b}$ invariant mass comes exclusively from the $\text{NLO}_{\text{prod}} \times \text{NLO}_{\text{dec}}$ contribution. On the other hand, for $m_{b\bar{b}} < m_H$ the NNLO corrections to the decay play a dominant role, increasing the distribution by about 40%, as compared to the $\mathcal{O}(20\%)$ increase from $\text{NLO}_{\text{prod}} \times \text{NLO}_{\text{dec}}$.

Next, we consider the transverse momentum of the $b\bar{b}$ system whose invariant mass provides the best approximation to the Higgs boson mass. The NNLO and approximate NNLO distributions for this observable are compared in Fig. 6; the cut $p_{\perp,W} > 150$ GeV is applied to events displayed in the right pane. It follows from Fig. 6 that the cut on the W boson transverse momentum re-shapes the distribution, pushing its maximum to larger values. Again, this is easily understood by observing that the $p_{\perp,W}$ cut implies the requirement $p_{\perp,b\bar{b}} > 150$ GeV at LO. In addition, if the cut on the W transverse momentum is applied, both the full and the approximate NNLO calculations develop a Sudakov shoulder below $p_{\perp,b\bar{b}} = p_{\perp,W}^{\text{cut}} = 150$ GeV. We note that this feature is somewhat less prominent in the full

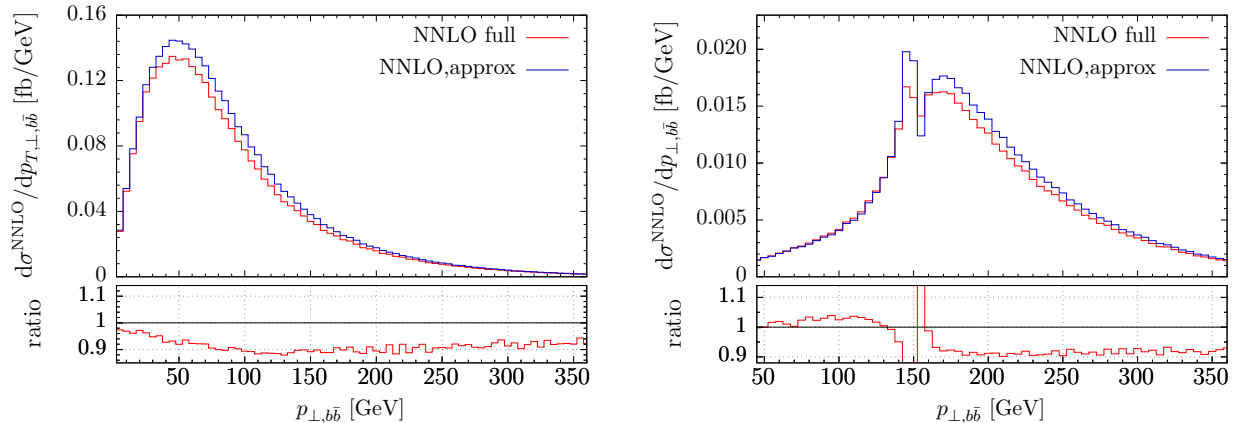


Figure 6: Same as Fig. 4, but for the transverse momentum of the $b\bar{b}$ system that is used to reconstruct the Higgs boson. See text for further details.

NNLO distribution.

To understand the relative impact of different contributions, we again split the full NNLO into two different parts, δ_{dec} and $\delta_{\text{NLO}\times\text{NLO}}$, and display them separately in Fig. 7. For values of $p_{\perp,b\bar{b}}$ larger than $p_{\perp,W}^{\text{cut}}$, the approximate NNLO is larger than the full NNLO by about $\mathcal{O}(5\% - 10\%)$, independent of whether or not the cut on the W boson transverse momentum is applied, due to the corrections from both $\text{NLO}_{\text{prod}} \times \text{NLO}_{\text{dec}}$ and the NNLO decay. When the $p_{\perp,W}$ cut is imposed, the slight increase at low values of $p_{\perp,b\bar{b}}$ is the result of a cancellation between the somewhat larger contributions from the NNLO decay and the $\text{NLO}_{\text{prod}} \times \text{NLO}_{\text{dec}}$. We also note that the $\text{NLO}_{\text{prod}} \times \text{NLO}_{\text{dec}}$ contribution smears the Sudakov shoulder.

It is also interesting to study the angular separation $\Delta R_{b\bar{b}} = \sqrt{\Delta\eta_{bb}^2 + \Delta\phi_{bb}^2}$ of the b - and \bar{b} -jets that are used to reconstruct the Higgs boson; the corresponding distributions without (left pane) and with (right pane) the $p_{\perp,W}$ cut are shown in Fig. 8. The impact of the W boson transverse momentum cut on the angular separation of the jets is dramatic, as the comparison of left and right panes shows. The shift to lower values of $\Delta R_{b\bar{b}}$ is again expected, as imposing the $p_{\perp,W}$ cut selects boosted Higgs kinematics whose decay products are closer together. Both with and without the $p_{\perp,W}$ cut, the NLO corrections modify the shape of $\Delta R_{b\bar{b}}$ distributions significantly, while the NNLO corrections have a much smaller impact.

Another distribution that is subject to large modifications if the cut on the vector boson

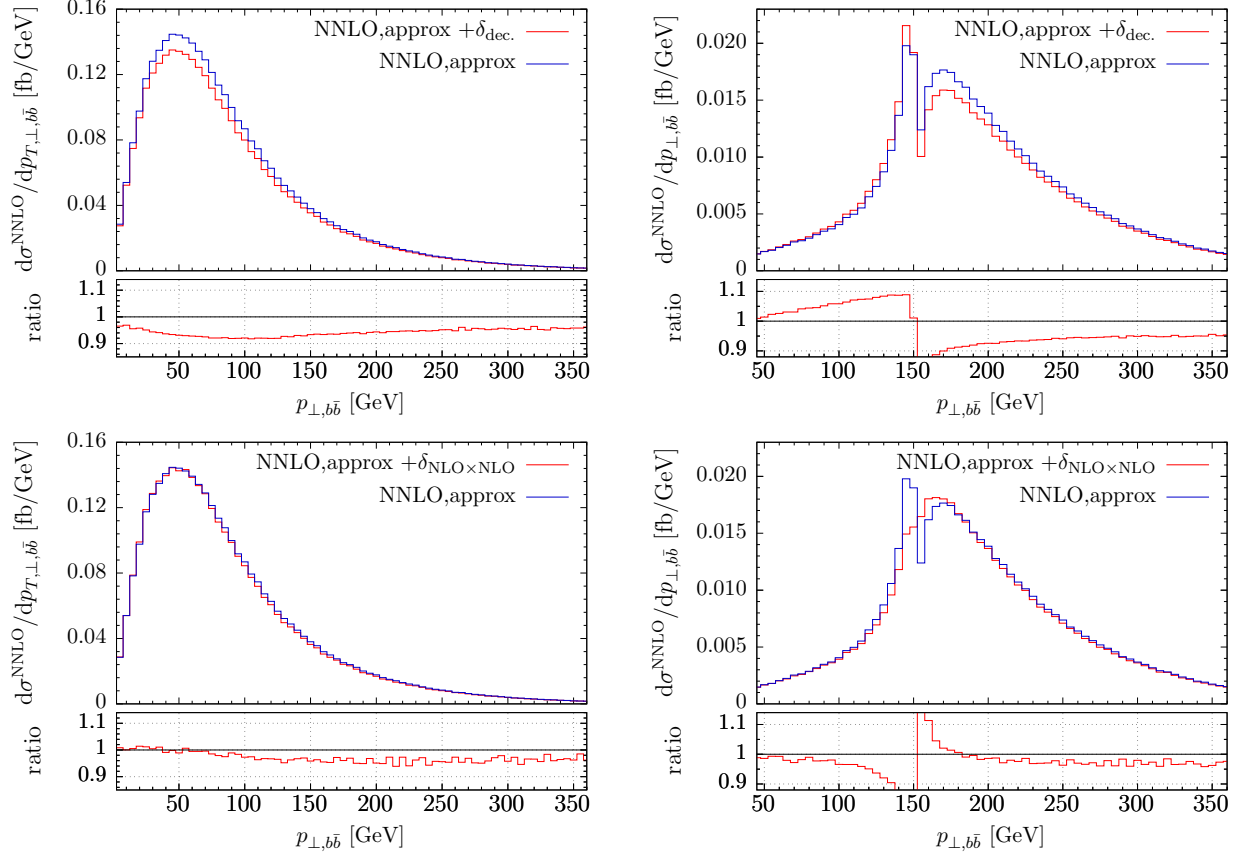


Figure 7: The different contributions to the distribution of the sum of transverse momenta of the b - and \bar{b} -jets that are used to reconstruct the Higgs boson. Left pane – without the p_{\perp}^W cut, right pane – with the $p_{\perp}^W > 150$ GeV cut. Upper row: only NNLO corrections to decay are included. Lower row: NLO corrections to the production and NLO corrections to the decay are included. See text for further details.

transverse momentum is applied is the transverse momentum distribution of the hardest b -jet; it is shown in Fig. 9. In this case, large radiative corrections appear below the value of the transverse momentum where the distribution reaches its maximum. If the p_{\perp}^W cut is not applied, large corrections at NLO are followed by moderate corrections at NNLO. On the contrary, if the p_{\perp}^W cut is in place, both the NLO and NNLO corrections are very large and perturbation theory does not appear to converge (see the right pane in Fig. 9). Clearly, the situation is completely different at high values of p_{\perp}^b where NNLO effects are relatively small and the NNLO/NLO K -factor is flat and close to one.

As the last example, we show in Fig. 10 the transverse momentum distribution of the charged

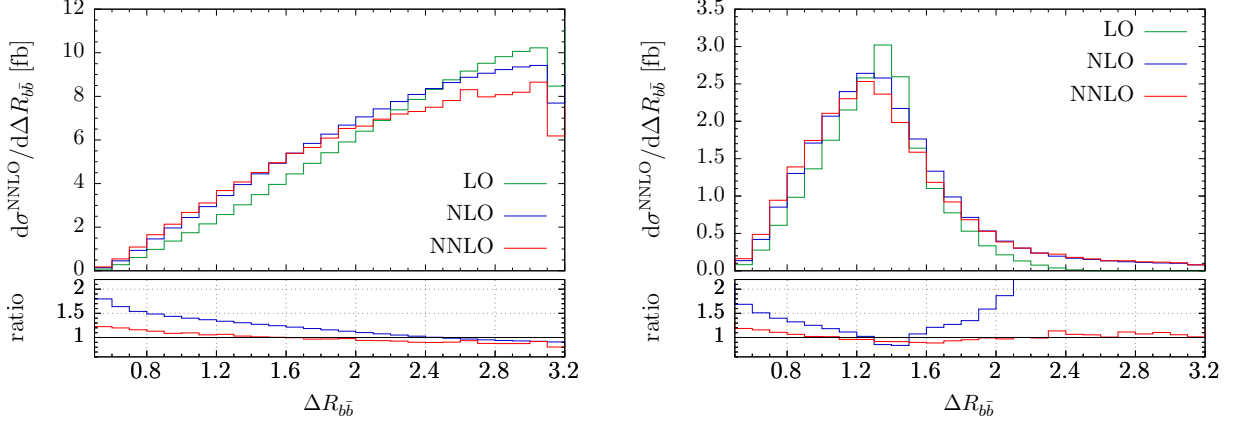


Figure 8: The $\Delta R_{b\bar{b}}$ distribution of the two b -jets used to reconstruct the Higgs boson. Left pane – without the p_{\perp}^W cut, right pane – with the $p_{\perp}^W > 150$ GeV cut. Lower panes – ratios of NLO and full NNLO to NLO distributions. See text for further details.

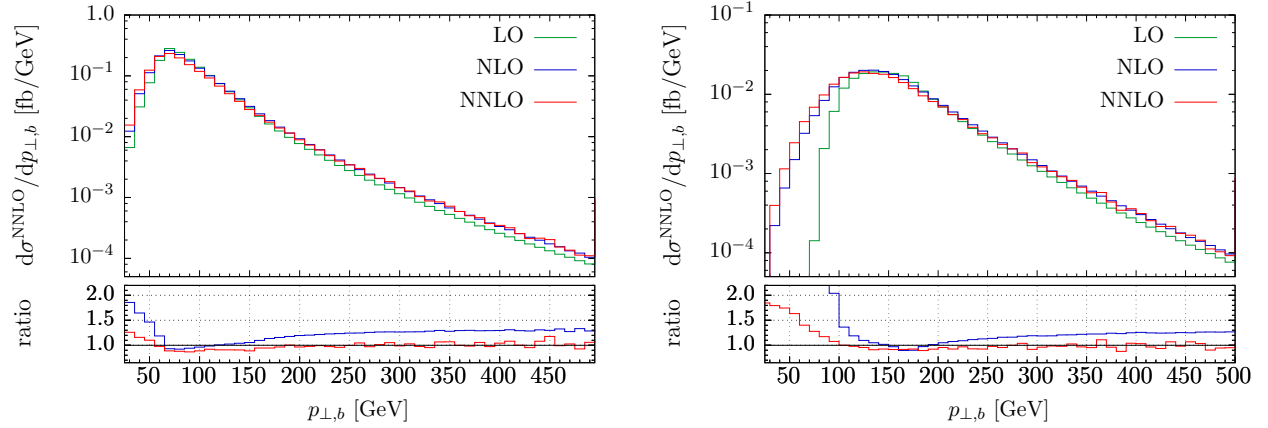


Figure 9: The transverse momentum of the hardest b - or \bar{b} -jet. Left pane – without the p_{\perp}^W cut, right pane – with the $p_{\perp}^W > 150$ GeV cut. Lower panes – ratios of NLO to LO and full NNLO to NLO distributions. See text for further details.

lepton that originates from the W decay. In this case, the cut on the W boson transverse momentum has a significant impact on the shape of the distribution, but the NLO and NNLO corrections to the two cases are very similar. In particular, the NNLO corrections in both cases are relatively small and do not change the shape of the respective NLO distributions.

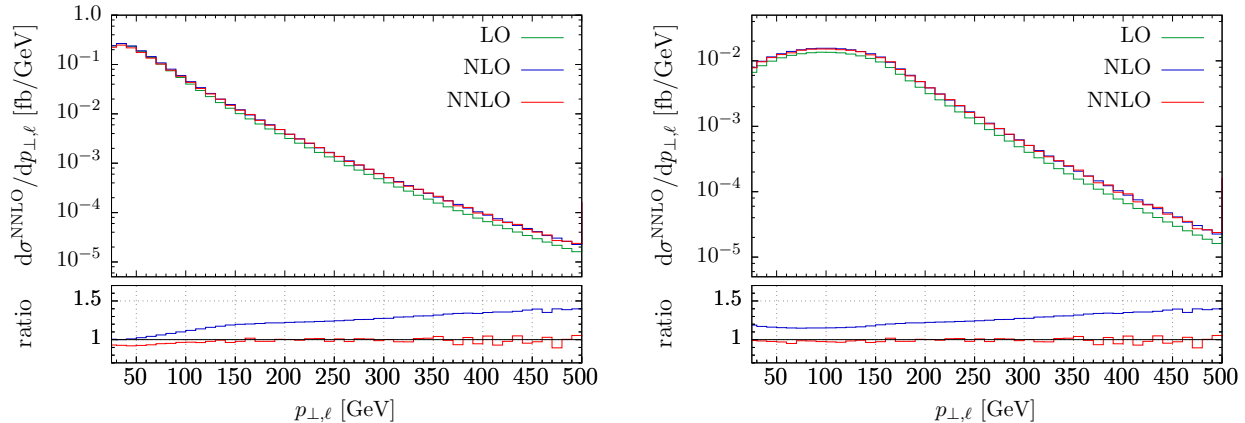


Figure 10: The transverse momentum distribution of the charged lepton. Left pane – without the p_{\perp}^W cut, right pane – with the $p_{\perp}^W > 150$ GeV cut. Lower panes – ratios of NLO to LO and NNLO to NLO distributions. See text for further details.

VI. COMPARISON OF FIXED ORDER AND PARTON SHOWER PREDICTIONS

The goal of this Section is to compare fixed order QCD predictions for $pp \rightarrow W(l\nu)H(b\bar{b})$, described in the previous Section, with the results obtained when parton showers are used to account for QCD radiation in $H \rightarrow b\bar{b}$ decays, as typically done in many experimental analyses. We use the publicly available HWJ generator [12] implemented in the POWHEG BOX framework [48–50] to compute the process $pp \rightarrow W(l\nu)H+j$ at NLO QCD accuracy. In order to be as close as possible to the NNLO calculation, and since the HWJ generator allows it, we run it with the improved MiNLO method [51, 52]. This allows observables that are inclusive in the production of the color-neutral system, i.e. quantities in which the jet is unresolved, to be computed with NLO QCD accuracy. Thus, the difference between the NNLO fixed order calculation and the NLO parton shower simulation for the process $pp \rightarrow W(l\nu)H$ is formally due only to the missing two loop amplitudes in the HWJ generator. The decay of the Higgs boson to a $b\bar{b}$ pair and an arbitrary number of gluons is instead simulated with a parton shower using PYTHIA-8 [53] with the default tune. Since we want to compare the parton shower results with a fixed order calculation, we do not include any non-perturbative effects in the simulation, i.e. the hadronization and the multi-parton interactions are switched off. In the parton shower simulation we reconstruct jets using the anti- k_t algorithm [54], and select b -jets according to Monte Carlo truth, in order to be as close as possible to experimental analyses. Following Ref. [22] and the analysis in the previous Section, we use

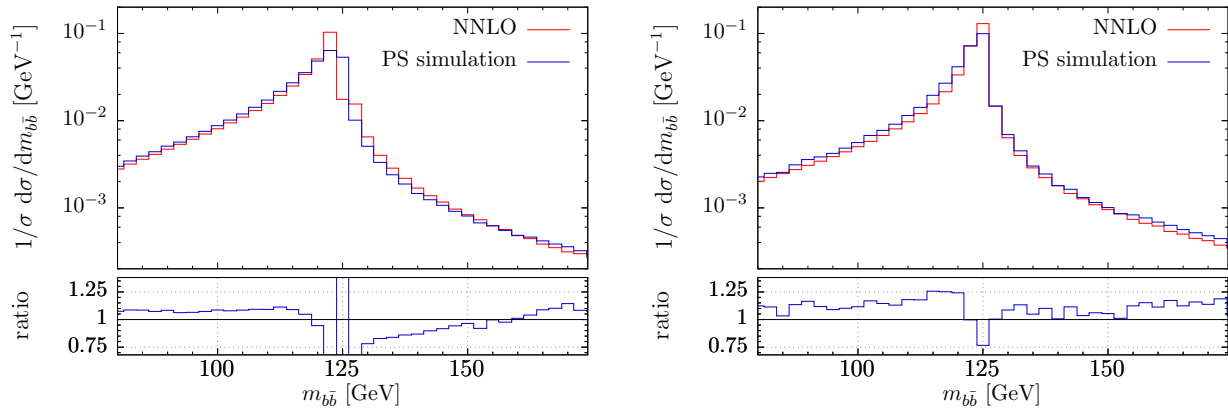


Figure 11: Comparison of fixed order and parton shower predictions for the normalized invariant mass distribution of the two b -jets used to reconstruct the Higgs boson. Left pane – without the p_{\perp}^W cut, right pane – with the $p_{\perp}^W > 150$ GeV cut. Lower panes – ratio of parton shower to fixed order predictions. See text for further details.

$R = 0.5$ for the jet radius.

As we have seen in the previous Section, radiative corrections to kinematic distributions in the $pp \rightarrow WH(b\bar{b})$ process exhibit non-trivial patterns, partially because of selection criteria that are applied to final state particles. In particular, large effects are observed for values of the $m_{b\bar{b}}$ invariant mass that are far from the value of the Higgs boson mass, or for values of the transverse momenta of the $b\bar{b}$ system or the leading b -jet that are below the cut on the transverse momentum of the W boson. All these kinematic regions have one thing in common – they are not populated *at all* if leading-order predictions are used. Hence, they require additional QCD radiation either in the production process or in the decay of the Higgs boson.

Moreover, some of these regions, e.g. $p_{\perp, b\bar{b}} \sim p_{\perp, W}^{\text{cut}}$ or hardest $p_{\perp, b} \rightarrow 0$, are close to kinematic boundaries where parton showers are known to accurately describe radiation effects. Other regions and observables, for example the case $m_{b\bar{b}} < m_H$ require a relatively hard gluon emission and it is unclear *a priori* if parton showers do a good job in describing them.

As in the previous Section, we study the b and \bar{b} jets whose invariant mass $m_{b\bar{b}}$ is closest to the Higgs mass. We show a comparison of the NNLO and parton shower predictions for the $m_{b\bar{b}}$ distribution in Fig. 11, for the transverse momentum distribution of the $b\bar{b}$ system in Fig. 12, and for the hardest b (or \bar{b}) jet p_{\perp} distribution in Fig. 13. In all of these cases, the

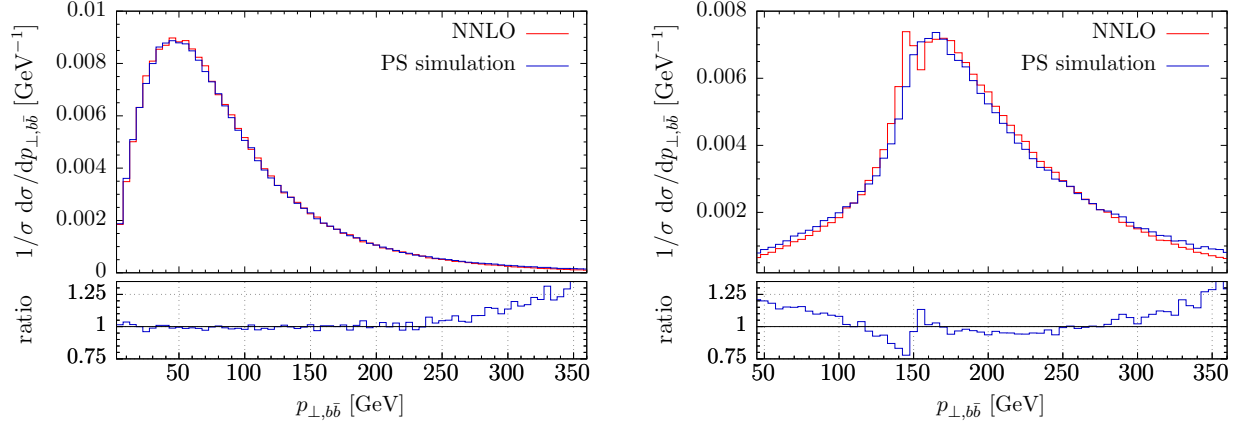


Figure 12: Same as Fig. 11 but for the transverse momentum of the $b\bar{b}$ system that is used to reconstruct the Higgs boson. See text for further details.

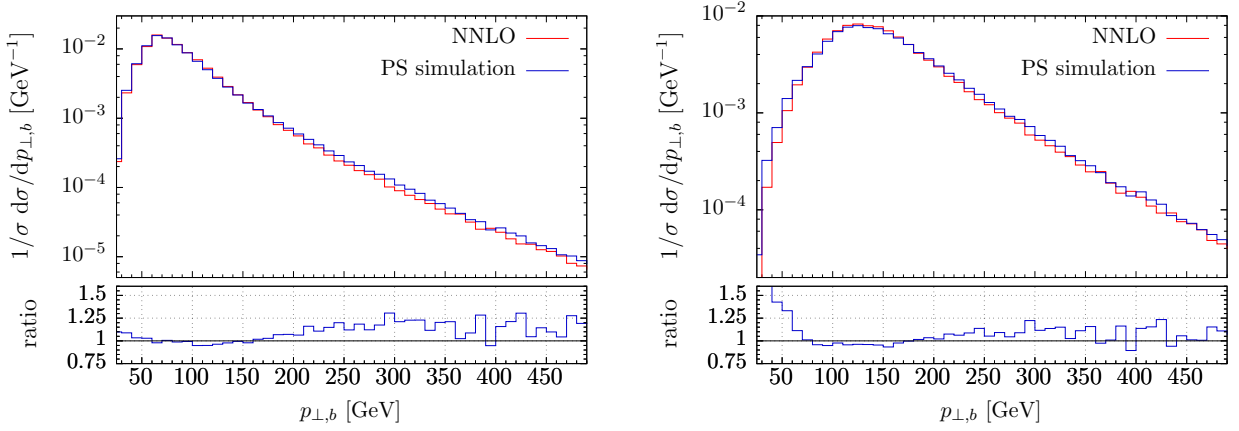


Figure 13: Same as Fig. 11 but for the hardest b (or \bar{b}) jet. See text for further details.

distributions are normalized to their inclusive result so that their shapes can be compared. However, we note that, while the fixed order and parton shower results use the same jet radius, the former makes use of the flavor- k_t jet algorithm while the latter uses the standard anti- k_t algorithm, and therefore the comparison between the two is not straightforward. We will return to this point at the end of this Section.

For the $m_{b\bar{b}}$ distribution, we observe that the parton shower does quite a good job in describing the NNLO corrections, although it predicts more events at both low and high values of $m_{b\bar{b}}$. Interestingly, the parton shower smears the peak at $m_{b\bar{b}} = m_H$ more significantly in the case where the $p_{\perp,W}$ cut is not applied. When this cut is imposed, the parton shower predicts fewer events at the peak but the smearing effect is not as dramatic.

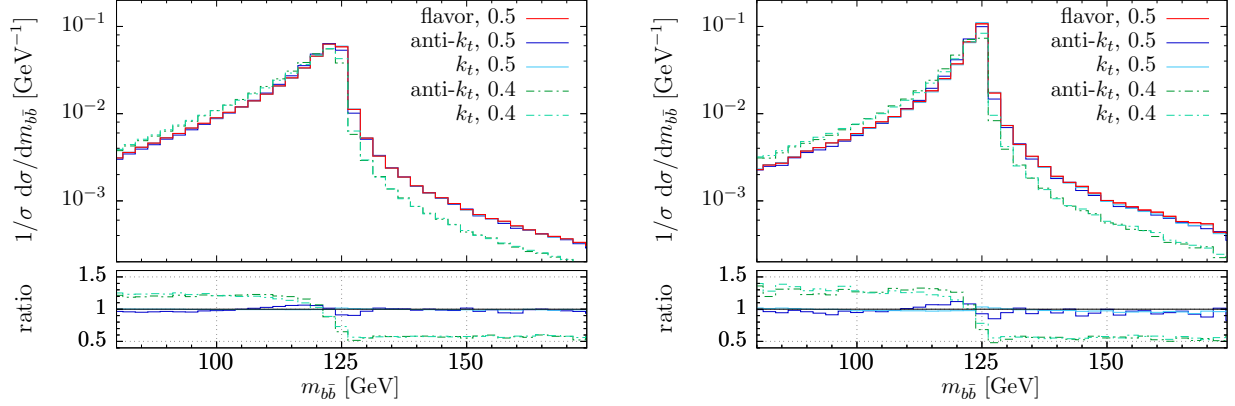


Figure 14: The invariant mass of a b -jet and a \bar{b} -jet that best approximates the Higgs boson mass, obtained from parton shower simulations with different jet algorithms and radii. Left pane – without the p_{\perp}^W cut, right pane – with the $p_{\perp}^W > 150$ GeV cut. Lower panes – ratio of results for the k_t and anti- k_t jet algorithms with $R = \{0.4, 0.5\}$ to the result for the flavor- k_t jet algorithm with $R = 0.5$. See text for further details.

Turning to the $p_{\perp, b\bar{b}}$ distribution, we observe that the parton shower is able to describe the NNLO distributions quite well. When the p_{\perp}^W cut is not imposed, the parton shower prediction is in excellent agreement with the fixed order one, except in the very high transverse momentum region. However, there is a difference at low $p_{\perp, b\bar{b}}$ if the p_{\perp}^W cut is applied, with the parton shower predicting more events in this region than the fixed order calculation. As expected, the parton shower also removes the Sudakov shoulder in this distribution that was observed in both the approximate and the full NNLO distributions.

Next, in Fig. 13 we show the p_{\perp} distribution of the b - (or \bar{b} -) jet with largest transverse momentum. Without the cut on p_{\perp}^W , the NNLO and shower results are similar, although the latter predicts slightly more events at large p_{\perp} . On the other hand, if the cut $p_{\perp}^W > 150$ GeV is imposed, the fixed order and shower calculations deviate significantly at small p_{\perp} . Large shower effects in this region are expected, since as we have shown in Section V, the fixed order predictions are not reliable here.

Given the different jet algorithms used in the fixed order and parton shower calculations, it is interesting to investigate to what extent the details of the jet definition affect these results. In Figs. 14 and 15, we show the invariant mass $m_{b\bar{b}}$ and transverse momentum distribution $p_{\perp, b\bar{b}}$, obtained from the parton shower simulation for different choices of the jet algorithm

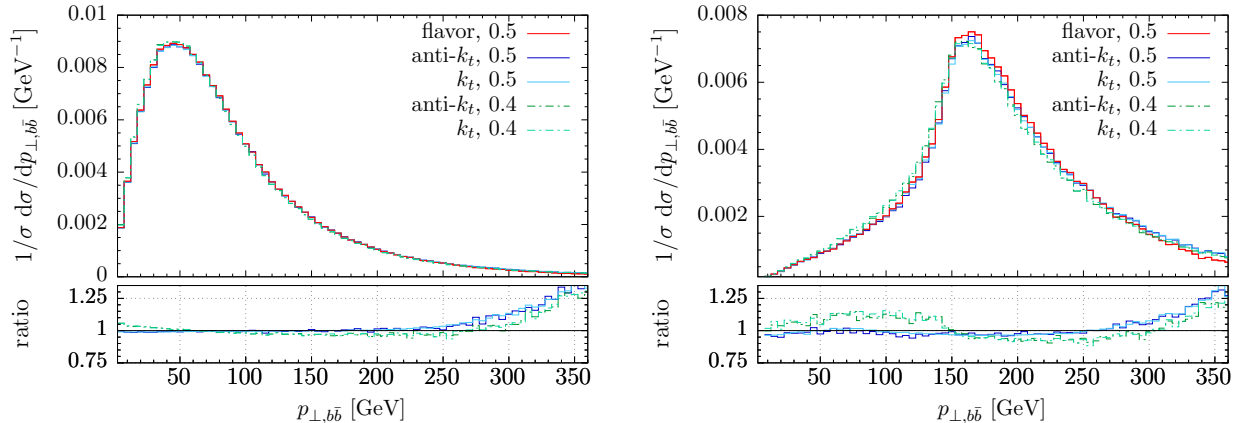


Figure 15: Same as Fig. 14 but for the transverse momentum of the $b\bar{b}$ system that is used to reconstruct the Higgs boson. See text for further details.

and radius. We compare the flavor- k_t jet algorithm [46] with both the k_t [55] and anti- k_t [54] algorithms. For the invariant mass distribution, Fig. 14 shows that both with and without the $p_{\perp}^W > 150$ GeV cut the result is quite insensitive to the recombination algorithm, and it only depends on the choice of the jet radius: smaller values of R lead to more events below the Higgs peak. For the $p_{\perp, b\bar{b}}$ on the other hand, Fig. 15 shows that without the p_{\perp}^W cut all jet algorithms and radii lead to the same result, apart from the high $p_{\perp, b\bar{b}}$ tail where the flavor- k_t jet algorithm [46] predicts fewer events compared to the k_t and anti- k_t cases. With the additional $p_{\perp}^W > 150$ GeV cut, a qualitative dependence on the jet radius similar to the one seen in the $m_{b\bar{b}}$ distribution is observed: smaller values of R lead to a softer spectrum.

VII. CONCLUSIONS

In this paper we presented a computation of the NNLO QCD corrections to the associated production of the Higgs boson $pp \rightarrow WH$ at the LHC. We considered the $H \rightarrow b\bar{b}$ decay of the Higgs boson and included radiative corrections to this decay through NNLO in perturbative QCD.

We pointed out an interesting contribution to Higgs decay to $b\bar{b}$ pairs that was ignored in previous *fully-differential* NNLO QCD computations to this process. This contribution is infrared-sensitive even after standard jets algorithms are applied and understanding it necessitates the computation of fully-differential NNLO corrections to the $H \rightarrow b\bar{b}$ decay

with massive bottom quarks. Although we argued that its numerical importance should be small, a more refined analysis is required to properly quantify these effects.

We found a number of kinematic distributions in the $pp \rightarrow W(l\nu)H(b\bar{b})$ process that receive large perturbative corrections if certain cuts on the final state, and especially a cut on the transverse momentum of the W boson, are applied. These findings are in accord with an earlier discussion given in Ref. [22].

We compared fixed order predictions for the $pp \rightarrow W(l\nu)H(b\bar{b})$ process with calculations where a parton shower is used to describe QCD radiation in $H \rightarrow b\bar{b}$ decay. Parton showers confirm the existence of large effects observed in fixed order computations. Since at the moment fixed order NNLO QCD computations for $H \rightarrow b\bar{b}$ are performed for massless b -quarks, one has to use specially-tailored jet algorithms to describe flavored jets in fixed order computations [46]. Although we showed in Section VI that the results are largely insensitive to the jet recombination algorithm, it would be interesting to repeat the fixed order studies reported here for the setup used in experimental analyses. This requires the computation of the fully-differential decay $H \rightarrow b\bar{b}$ through NNLO QCD keeping the full dependence on the b -quark mass. It would also be interesting to compare fixed order predictions to more advanced parton shower implementations, as described e.g. in Refs. [20, 56–58]. We leave these investigations for future work.

Acknowledgments We would like to thank Munich Institute for Astronomy and Particle Physics (MIAPP) for hospitality and partial support during the programs *Automated, Resummed and Effective* and *Mathematics and physics of scattering amplitudes*. The research of K.M. and R.R. is partially supported by BMBF grant 05H15VKCCA. The research of F.C. was supported in part by the ERC starting grant 637019 “MathAm”. We are grateful to G. Salam for interesting discussions and for providing us with a private implementation of the flavor- k_t jet algorithm [46]. We are indebted to F. Tramontano for discussions and for his help in comparison with the results of Ref. [22].

[1] G. Aad *et al.* [ATLAS Collaboration], JHEP **1501**, 069 (2015).

[2] The ATLAS collaboration [ATLAS Collaboration], ATLAS-CONF-2016-091.

[3] S. Chatrchyan *et al.* [CMS Collaboration], Phys. Rev. D **89**, no. 1, 012003 (2014).

- [4] M. Aaboud *et al.* [ATLAS Collaboration], JHEP **1712**, 024 (2017).
- [5] J. Ellis, V. Sanz and T. You, Eur. Phys. J. C **73**, 2507 (2013).
- [6] J. M. Butterworth, A. R. Davison, M. Rubin and G. P. Salam, Phys. Rev. Lett. **100**, 242001 (2008).
- [7] G. Aad *et al.* [ATLAS and CMS Collaborations], JHEP **1608**, 045 (2016).
- [8] T. Han and S. Willenbrock, Phys. Lett. **B273**, 167 (1990); H. Baer, B. Bailey and J. F. Owens, Phys. Rev. D **47**, 2730 (1993); J. Ohnemus and W. J. Stirling, Phys. Rev. D **47**, 2722 (1993); S. Mrenna and C. P. Yuan, Phys. Lett. B **416**, 200 (1998); M. Spira, Fortsch. Phys. **46**, 203 (1998); A. Djouadi and M. Spira, Phys. Rev. D **62**, 014004 (2000).
- [9] M. L. Ciccolini, S. Dittmaier and M. Kramer, Phys. Rev. D **68**, 073003 (2003).
- [10] A. Denner, S. Dittmaier, S. Kallweit and A. Muck, JHEP **1203**, 075 (2012).
- [11] S. Frixione and B. Webber, [hep-ph/0506182]; K. Hamilton, P. Richardson and J. Tully, JHEP **0904**, 116 (2009); F. Granata, J. M. Lindert, C. Oleari and S. Pozzorini, JHEP **1709**, 012 (2017).
- [12] G. Luisoni, P. Nason, C. Oleari and F. Tramontano, JHEP **1310**, 083 (2013).
- [13] O. Brein, A. Djouadi and R. Harlander, Phys. Lett. B **579**, 149 (2004).
- [14] R. Hamberg, W. L. van Neerven and T. Matsuura, Nucl. Phys. B **359**, 343 (1991) Erratum: [Nucl. Phys. B **644**, 403 (2002)].
- [15] R. V. Harlander and W. B. Kilgore, Phys. Rev. Lett. **88**, 201801 (2002).
- [16] O. Brein, R. Harlander, M. Wiesemann and T. Zirke, Eur. Phys. J. C **72**, 1868 (2012).
- [17] O. Brein, R. V. Harlander and T. J. E. Zirke, Comput. Phys. Commun. **184**, 998 (2013).
- [18] G. Ferrera, M. Grazzini and F. Tramontano, Phys. Rev. Lett. **107**, 152003 (2011).
- [19] J. M. Campbell, R. K. Ellis and C. Williams, JHEP **1606**, 179 (2016).
- [20] W. Astill, W. Bizon, E. Re and G. Zanderighi, JHEP **1606**, 154 (2016).
- [21] G. Ferrera, M. Grazzini and F. Tramontano, JHEP **1404**, 039 (2014).
- [22] G. Ferrera, G. Somogyi and F. Tramontano, arXiv:1705.10304 [hep-ph].
- [23] V. Del Duca, C. Duhr, G. Somogyi, F. Tramontano and Z. Trocsanyi, JHEP **1504**, 036 (2015).
- [24] C. Anastasiou, F. Herzog and A. Lazopoulos, JHEP **1203**, 035 (2012).
- [25] F. Caola, K. Melnikov and R. Röntsch, Eur. Phys. J. C **77**, no. 4, 248 (2017).
- [26] M. Czakon, Phys. Lett. B **693**, 259 (2010).
- [27] M. Czakon, Nucl. Phys. B **849**, 250 (2011).

- [28] W. T. Giele and E. W. Glover, Phys. Rev. D **46**, 1980 (1992); W. T. Giele, E. W. Glover and D. A. Kosower, Nucl. Phys. B **403**, 633 (1993).
- [29] S. Catani and M. H. Seymour, Nucl. Phys. B **485**, 291 (1997) [Erratum-ibid. B **510**, 503 (1998)].
- [30] S. Frixione, Z. Kunszt and A. Signer, Nucl. Phys. B **467**, 399 (1996).
- [31] S. Frixione, Nucl. Phys. B **507**, 295 (1997).
- [32] A. Gehrmann-De Ridder, T. Gehrmann and E. W. N. Glover, JHEP **0509**, 056 (2005); Phys. Lett. B **612**, 36 (2005); Phys. Lett. B **612**, 49 (2005); A. Daleo, T. Gehrmann and D. Maitre, JHEP **0704**, 016 (2007); A. Daleo, A. Gehrmann-De Ridder, T. Gehrmann and G. Luisoni, JHEP **1001**, 118 (2010); T. Gehrmann and P. F. Monni, JHEP **1112**, 049 (2011); R. Boughezal, A. Gehrmann-De Ridder and M. Ritzmann, JHEP **1102**, 098 (2011); A. Gehrmann-De Ridder, T. Gehrmann and M. Ritzmann, JHEP **1210**, 047 (2012); J. Currie, E. W. N. Glover and S. Wells, JHEP **1304**, 066 (2013).
- [33] M. Czakon and D. Heymes, Nucl. Phys. B **890**, 152 (2014).
- [34] R. Boughezal, C. Focke, X. Liu and F. Petriello, Phys. Rev. Lett. **115**, no. 6, 062002 (2015).
- [35] J. Gaunt, M. Stahlhofen, F. J. Tackmann and J. R. Walsh, JHEP **1509**, 058 (2015).
- [36] S. Catani and M. Grazzini, Phys. Rev. Lett. **98**, 222002 (2007); M. Grazzini, JHEP **0802**, 043 (2008).
- [37] M. Cacciari, F. A. Dreyer, A. Karlberg, G. P. Salam and G. Zanderighi, Phys. Rev. Lett. **115**, no. 8, 082002 (2015).
- [38] V. Del Duca, C. Duhr, A. Kardos, G. Somogyi and Z. Trocsanyi, Phys. Rev. Lett. **117**, no. 15, 152004 (2016); V. Del Duca, C. Duhr, A. Kardos, G. Somogyi, Z. Szor, Z. Trocsanyi and Z. Tulipant, Phys. Rev. D **94**, no. 7, 074019 (2016).
- [39] R. Boughezal, K. Melnikov and F. Petriello, Phys. Rev. D **85**, 034025 (2012).
- [40] R. D. Ball *et al.* [NNPDF Collaboration], JHEP **1504**, 040 (2015).
- [41] D. de Florian *et al.* [LHC Higgs Cross Section Working Group], doi:10.23731/CYRM-2017-002 arXiv:1610.07922 [hep-ph].
- [42] J. Davies, M. Steinhauser and D. Wellmann, Nucl. Phys. B **920**, 20 (2017).
- [43] E. Braaten and J. P. Leveille, Phys. Rev. D **22**, 715 (1980).
- [44] S. Catani and M. Grazzini, Nucl. Phys. B **570**, 287 (2000).
- [45] P. A. Baikov, K. G. Chetyrkin and J. H. Kühn, Phys. Rev. Lett. **96**, 012003 (2006).

- [46] A. Banfi, G. P. Salam and G. Zanderighi, *Eur. Phys. J. C* **47**, 113 (2006).
- [47] M. Cacciari, G. P. Salam and G. Soyez, *Eur. Phys. J. C* **72**, 1896 (2012).
- [48] P. Nason, *JHEP* **0411**, 040 (2004).
- [49] S. Frixione, P. Nason and C. Oleari, *JHEP* **0711**, 070 (2007).
- [50] S. Alioli, P. Nason, C. Oleari and E. Re, *JHEP* **1006**, 043 (2010).
- [51] K. Hamilton, P. Nason and G. Zanderighi, *JHEP* **1210**, 155 (2012).
- [52] K. Hamilton, P. Nason, C. Oleari and G. Zanderighi, *JHEP* **1305**, 082 (2013).
- [53] T. Sjostrand, S. Mrenna and P. Z. Skands, *Comput. Phys. Commun.* **178**, 852 (2008).
- [54] M. Cacciari, G. P. Salam and G. Soyez, *JHEP* **0804**, 063 (2008).
- [55] S. Catani, Y. L. Dokshitzer, M. H. Seymour and B. R. Webber, *Nucl. Phys. B* **406**, 187 (1993) and refs. therein; S. D. Ellis and D. E. Soper, *Phys. Rev. D* **48**, 3160 (1993).
- [56] P. Richardson and D. Winn, *Eur. Phys. J. C* **72**, 2178 (2012).
- [57] S. Höche, Y. Li and S. Prestel, *Phys. Rev. D* **91**, no. 7, 074015 (2015).
- [58] S. Alioli, C. W. Bauer, C. Berggren, F. J. Tackmann and J. R. Walsh, *Phys. Rev. D* **92**, no. 9, 094020 (2015).